Computational Materials Science 165 (2019) 121–128

Contents lists available at ScienceDirect

Computational Materials Science

journal homepage: www.elsevier.com/locate/commatsci

First-principles study on the two-dimensional siligene (2D SiGe) as an anode material of an alkali metal ion battery

Arindam Sannyal[a], Yoonho Ahn[b,*], Joonkyung Jang[a,*]

[a] Department of Nanoenergy Engineering, Pusan National University, Busan 46241, Republic of Korea
[b] School of Liberal Arts, Korea University of Technology and Education, Cheonan 31253, Republic of Korea

ARTICLE INFO

Keywords:
Alkali metal ion battery
Density functional theory
Two-dimensional materials
Siligene
Storage capacity
Voltage

ABSTRACT

By using the density functional theory, we propose that the two-dimensional (2D) SiGe is a promising anode material of a sodium or potassium ion battery. We confirm the thermal and dynamic stabilities of the SiGe sheet by calculating the formation energy and phonon dispersion, respectively. The SiGe sheet provides moderate/low migration energy barriers for the alkali metal atoms (0.14–0.35 eV), suggesting fast charge/discharge rates. The SiGe sheet gives high theoretical capacities (for Li/K ~ 532 mA h g^{-1} and for Na ~ 1064 mA h g^{-1}) and stable voltage profiles.

1. Introduction

Owing to the low abundance and high cost of lithium (Li), it is highly desired to develop alternative secondary battery systems [1,2]. Sodium-ion batteries (NIBs) and potassium-ion batteries (KIBs) are thus extensively studied because of their higher abundances and similar intercalation chemistries [3–5]. Designing an anode material with a robust electrochemical performance is a major challenge in developing such a battery [6,7]. The conventional graphite anode of lithium-ion battery (LIB) cannot be used for NIB or KIB, because of the slow Na/K intercalation into graphite which leads to a slow charge–discharge rate [8,9].

In this regard, anode materials made of silicon (Si) and germanium (Ge) emerge as potential candidates due to their high specific capacities [10,11] and low working potentials [12,13]. However, commercialization of the bulk Si or Ge anode is hampered by the excessive volume change during the metal insertion-deinsertion process which gives poor reversibility and safety issues [13]. Enhanced properties might be obtained by combining two elements Si and Ge [14–16]. Due to elevated electrical conductivity and Li diffusivity of Ge, it is believed that integrating Ge with Si can improve the diffusivity of Li and electronic conductivity of Si [12,17,18]. Moreover, in SiGe alloy, Li reacts with Si and Ge at different potentials [12,19]. Consequently, when Li inserts into Si, Ge can buffer the volume change of the Si [12,19,20]. Porous micro- and nano-particles of the alloy of SiGe were shown to serve as anode materials for LIBs with high reversible capacities [12,18,19,21–23]. However, the nanoporous SiGe alloys were obtained by complex multistep methods with low production efficiency, hindering their large-scale industrial production [18,21–23].

On the other hand, two-dimensional (2D) materials, due to their high surface areas, recently have been considered for anode materials, including phosphorus (P) [24,25], boron (B) [26,27], Si [28,29], Ge [30,31], and tin (Sn)-based anodes [32,33]. Theoretical studies revealed that the 2D sheet of Si (silicene) does not suffer from an irreversible structural change during the lithium insertion [34]. The density functional theory (DFT) calculations proposed that a sheet of Si or Ge (germanene) can deliver high capacities for Li- and Na-ion batteries [35,36]. Unfortunately, the 2D sheets of Si and Ge are unstable under the ambient conditions however, making these materials inapplicable to real batteries [37,38].

A graphene-like structure of SiGe (siligene) was recently studied by using the *ab initio* calculation and found to be energetically more stable than the 2D Ge [39,40]. The buckled geometrical structure of SiGe sheet gave electronic band structures similar to those found for graphene. Significantly, within the sheet of SiGe, the Si atom has a higher degree of hydrogenation than that of the Ge atom [41]. Consequently, the electronic structure of the SiGe sheet can be tuned by controlling the coverage of hydrogen. The tunable electromagnetic properties of the SiGe sheet opens up the applications of the 2D SiGe in electronic devices [39].

Considering the promising optical features of the 2D SiGe, we here study the suitability of the 2D SiGe as an anode material of LIB, NIB, or KIB. By performing DFT calculations, we show the 2D SiGe sheet is both thermally and dynamically stable. The SiGe sheet possessed low

* Corresponding authors.
E-mail addresses: yhahn@koreatech.ac.kr (Y. Ahn), jkjang@pusan.ac.kr (J. Jang).

https://doi.org/10.1016/j.commatsci.2019.04.039
Received 22 March 2019; Accepted 22 April 2019

diffusion barriers (0.14–0.35 eV) and low open-circuit voltages (1.08–1.38 V). Moreover, the sheet of SiGe yielded high capacities of 1064 mA h g^{-1} for Na and 532 mA h g^{-1} for K, which are much higher than those of the other 2D anode materials reported. We unraveled physical insights for the adsorption behaviors of alkali metals on the 2D SiGe. Thereby, we propose that the 2D sheet of SiGe is a promising anode material of a NIB or KIB.

2. Computational methods

The electron-ion interactions were calculated by using the projector-augmented wave (PAW) method [42]. The generalized gradient approximation (GGA) of the Perdew–Burke–Ernzerhof (PBE) functional was used for the exchange-correlation [43]. We used the plane-wave cutoff energy of 520 eV in the expansion of the valence electron wave function. The van der Waals interaction was taken into account by using the semi-empirical correction scheme of Grimme (DFT + D2) [44] which successfully described the adsorption and diffusion of lithium in graphite [45]. The adsorption and diffusion of metal ions on the 2D SiGe sheet were modeled by using a 4 × 4 × 1 slab. We used a vacuum spacing of 20 Å along the Z-direction to remove the fictitious self-interaction of the supercell and its periodic images. For the purpose of evaluating the theoretical capacities and voltage profiles, we used a 3 × 3 × 1 sheet of SiGe. The convergence criteria for the energy and force were taken to be < 10^{-5} eV and < 0.01 eV $Å^{-1}$, respectively.

We calculated the phonon dispersion spectra to evaluate the dynamic stability of the SiGe sheet by using the Phonopy code [46]. In the geometry optimizations, the Brillouin zones of the 2D and bulk SiGe were sampled using 3 × 3 × 1 and 3 × 3 × 2 Monkhorst-Pack [47] k-point meshes, respectively. In calculating the density of states (DOSs) and band structures, we used a denser k-point mesh (9 × 9 × 1). We calculated the difference in charge density by the Bader charge analysis [48–50]. The minimum energy paths were constructed by using the climbing image nudged elastic band (CI-NEB) method [51,52]. Five intermediate images were considered for the CI-NEB calculation. All the electronic structure calculations were executed using the Vienna ab initio simulation package (VASP) [53,54].

3. Results and discussion

3.1. Structure of SiGe sheet

The lattice constants of the bulk SiGe were calculated as a = 3.88 Å and c = 6.40 Å. The lattice parameter of the 2D SiGe was a = 3.91 Å, agreeing with the previous DFT studies [39,40] with deviations less than 1%. Unlike the planar graphene, the sheet of SiGe had a hexagonal buckled structure in which Si and Ge atoms were alternately placed in two sublattices (Fig. 1). The buckling amplitude (Δ) of the 2D SiGe was 0.58 Å, less than that (0.81 Å) of the bulk SiGe. The Si-Ge bond length of the 2D SiGe was 2.34 Å, which is longer than the Si-Si bond length (2.28 Å) in silicene but shorter than the Ge-Ge bond length (2.40 Å) in germanene [39]. The lattice constant and buckling amplitude of the 2D SiGe (a = 3.91 Å and Δ = 0.58 Å) were between the corresponding values of silicene (a = 3.86 Å and Δ = 0.42 Å) and germanene (a = 4.03 Å and Δ = 0.67 Å) [39,40].

We calculated the formation energy of the 2D SiGe, E_f, as

$$E_f = E_{SiGe} - E_{Si} - E_{Ge}, \quad (1)$$

where E_{SiGe}, E_{Si}, and E_{Ge} are the energies of the SiGe sheet, of a single Si atom in the bulk, and of a single Ge atom in the bulk, respectively. The negative formation energy (−1.51 eV per unit cell) confirmed the thermodynamic stability of the 2D SiGe. We ignored the entropy effect which should be negligible at room temperature [31]. The dynamic stability of the sheet of SiGe was checked by constructing the phonon dispersion spectra using the density functional perturbation theory (DFPT) [55]. The absence of an imaginary frequency in the phonon spectra (Fig. 1c) proved the vibrational stability of the sheet of SiGe.

3.2. Adsorption of alkali metal atom on the sheet of SiGe

An undesirable formation of a metal cluster will not occur if metal atoms strongly bind to an electrode material [56]. Therefore, we studied the binding of a metal atom on the SiGe sheet. We found four most favorable binding sites as illustrated in Fig. 1a: sites above the center of the hexagonal ring (site H), above the Si atom (site T_{Si}), above the Ge atom (site T_{Ge}), and above the midpoint of the Si-Ge bond (site B). We defined the adsorption energy of an alkali metal atom M (=Li/Na/K), E_{ads}, as

$$E_{ads} = E_{MSiGe} - E_{SiGe} - E_M, \quad (2)$$

where E_{MSiGe} and E_{SiGe} are the total energies of the metal-adsorbed sheet of SiGe and of the pristine SiGe sheet, respectively, and E_M is the energy per metal atom in their bulk. By definition, the more negative is E_{ads}, the stronger is the adsorption. In the adsorption process, a metal atom moved from site B to the top of the nearest Si atom (T_{Si}) (Fig. S1), showing that a metal atom cannot be adsorbed at site B. Table 1 lists E_{ads}s for different binding sites. The binding at site H was the strongest because of its high coordination number [30,57]. The E_{ads}s of Li, Na, and K atoms at site H were −0.85, −0.84, and −1.24 eV, respectively.

The adsorption of a metal atom on the sheet of SiGe was further analyzed by calculating the difference in the charge density, Δρ, defined as

$$\Delta\rho = \rho_{MSiGe} - \rho_{SiGe} - \rho_M, \quad (3)$$

where ρ_{MSiGe}, ρ_{SiGe}, and ρ_M are the charge density values of the metal-adsorbed and pristine sheets of SiGe and of a single metal atom, respectively. Fig. 2 illustrates Δρ for the metal atoms adsorbed at site H, showing a significant electron transfer from metal to SiGe. The Bader charge analysis showed that the Li, Na, and K atoms donate 0.87*e*, 0.85*e*, and 0.94*e* to the substrate, respectively. The metal atoms thus

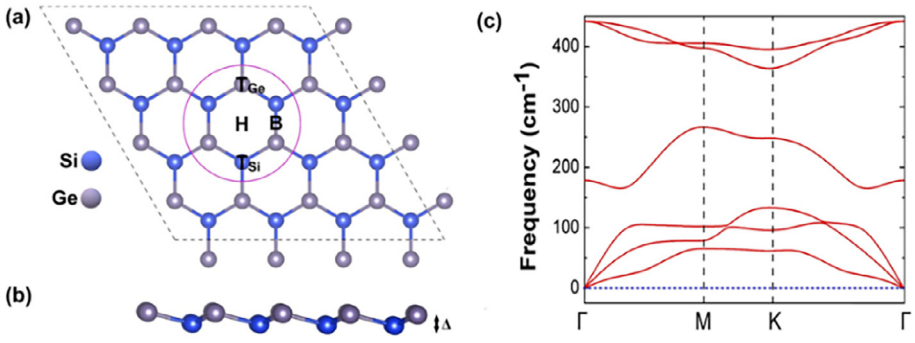

Fig. 1. (a) Top and (b) side views of the optimized structure of the 2D SiGe. The unit cell is marked with a circle and different binding sites are denoted by labels H, T_{Ge}, T_{Si}, and B. (c) Phonon dispersion curves calculated for the 2D SiGe sheet.

Table 1
Adsorption energies of alkali metal atoms E_{ads}s (in eV) at three different binding sites of the SiGe sheet (Fig. 1a). Also listed are metal-to-SiGe charge transfers $\Delta\rho$s at H sites (Fig. 1b) calculated by using the Bader charge analysis.

Metal	Adsorption energy (eV)			$\Delta\rho^H$ (IeI)
	H	T_{Si}	T_{Ge}	
Li	−0.85	−0.55	−0.25	0.87
Na	−0.84	−0.65	−0.40	0.85
K	−1.24	−1.12	−0.91	0.94

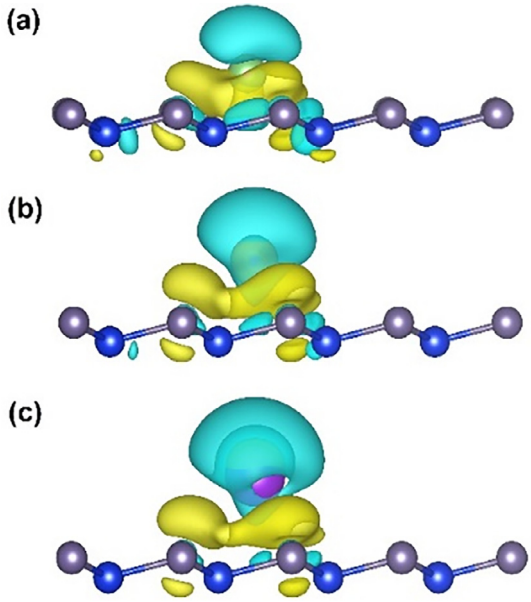

Fig. 2. Difference in the charge of the 2D SiGe adsorbed with a single Li (a), Na (b), or K (c) atom. The cyan and yellow areas represent electron loss and gain, respectively. The isosurface value is set to 0.001 IeI bohr^{-3}.

existed in virtually cationic states and were chemically bonded to the sheet of SiGe. These $\Delta\rho$s indicate that the binding of K is stronger than that of Li or Na.

An anode material should have a good electrical conductivity for fast electrochemical reactions during the charge and discharge cycles. We, therefore, investigated the electronic DOSs and the band structure of the 2D SiGe upon adsorption of metal. We found that the 2D SiGe possesses the Dirac cone-shaped band dispersion at the 'K' point with a band gap of 12 meV (Fig. S2), as found in the previous theoretical study [40]. Similar Dirac-cones at K point were observed in the conventional Dirac-fermion materials such as graphene [58,59], silicene [60,61], and germanene [61,62]. The partial DOSs (PDOSs), drawn in Fig. 3, show that the DOS in the vicinity of the Fermi level is equally contributed by Si and Ge atoms, indicating that the Dirac cone is a mixture of Si and Ge states [40]. The metal-to-SiGe charge transfer effectively shifted the Fermi energy level into the conduction band. The adsorption of a single metal atom thus enhanced the electrical conductivity of the semiconducting sheet of SiGe. Similar behavior was observed for other anode materials, such as phosphorene [24,25], group-IV monochalcogenides [30,56], and boron phosphide [26].

We studied the electronic structure of the 2D sheet of SiGe with increasing the concentration of metal. At a low coverage of Li, electrons transferred from Li atoms to the sheet of SiGe, rendering a metallic state of Li_xSiGe (Fig. S3a). Upon full lithiation ($Li_{2.0}$SiGe) however, electrons transferred from SiGe to the layer of Li (Fig. 4a). Resultingly, the band gap of the 2D SiGe widened from 0.012 eV to 0.98 eV, which is undesirable for application in LIBs. The prior theoretical studies showed that the poor electronic conductivities of the sheets of phosphorene [63] and SnS_2 [64] can be enhanced by introducing graphene sheets. The heterostructure of SiGe and graphene might solve the present inferior electrical conductivity, but this needs experimental verification. By contrast, the full adatom adsorption of Na and K increased the total DOS around the Fermi level (Fig. S3). In these cases, the band gaps disappeared at the Fermi level, implying that these structures will give metallic electronic responses.

3.3. Diffusion of Li/Na/K atom on 2D SiGe

For a fast charging and discharging [65,66], metal atoms should be highly mobile on the sheet of SiGe. We studied the diffusions of metal atoms between two neighboring centers of the hexagonal rings (H sites) of the 2D SiGe. We found three pathways for migration of metal atoms (Fig. 5a): one directly through the bond between Si and Ge atoms (Path-1), one through the top of Si atom (Path-2), and one through the top of Ge atom (Path-3). Upon optimization, metal atoms deviated from the straight Path-1 and switched to Path-2 eventually. This arose from that, during the surface loading process, metal atoms diffused from the bridge position to the top of the Si atom, as found in the adsorption process (Fig. S1). Metal atoms, therefore, followed the zigzag pathways (Path-2 and Path-3).

The energy profiles of Path-2 (H_1-T_{Si}-H_2) and Path-3 (H_1-T_{Ge}-H_2) are shown in Fig. 5b and c, respectively. In Path-2, metal atom encountered two energy barriers of the same height separated by a metastable site (T_{Si}). The energy barriers for the diffusions of Li, Na, and K atoms were 0.35, 0.21, and 0.14 eV, respectively. On the other hand, the activation energies for Path-3 were 0.60, 0.43, and 0.34 eV for Li, Na, and K, respectively, which are higher than those for Path-2. In Path-3, the diffusion of Li faced two energy barriers separated by a metastable state, but the diffusions of Na and K atoms had a single energy barrier without any metastable state. This is attributed to the larger atomic radii of Na and K. We estimated diffusion constant, D, by using the Arrhenius equation [24,67],

$$D \approx \exp\left(-\frac{E_a}{k_B T}\right), \tag{4}$$

where k_B and E_a are the Boltzmann constant and activation energy, respectively. According to Eq. (4), Li, Na, and K atoms diffuse along Path-2 1.69×10^4, 5.25×10^3, and 2.41×10^3 times faster, respectively, than along Path-3 at room temperature. In both pathways, the energy barrier for diffusion decreased with increasing the atomic number of metal. Na and K atoms, having larger atomic radii, were placed at distances longer than that of Li from the surface of SiGe and thus experienced less attraction from SiGe. The present energy barriers of diffusion are lower than those of Si_2BN (0.32–0.48 eV) [28], MoN_2 (0.49–0.78 eV) [68], Si (0.57 eV) [69], and TiO_2 (~0.65 eV) [70,71] but comparable to those of other layered anode materials such as TiS_3 (0.26–0.35 eV) [72], TiC_3 (0.18 eV) [73], and popgraphene (0.37 eV) [74].

3.4. Voltage and theoretical capacity

The storage performance of the SiGe sheet was evaluated by studying the concentration-dependent adsorption behavior of metal atoms. Note both sides of the 2D SiGe can be adsorbed with metal atoms. The adsorption energy of metal atoms in the n^{th} layer, E_{ave}, (on both sides of SiGe) was given by

$$E_{ave} = \frac{E(M_{18n}SiGe) - E(M_{18(n-1)}SiGe) - 18E_M}{18}, \tag{5}$$

where $E(M_{18n}SiGe)$ and $E(M_{18(n-1)}SiGe)$ are the total energies of SiGe sheets adsorbed with n and $n-1$ layers of metal atoms, respectively, and E_M is the energy per atom of the bulk metal. E_{ave} indicates whether the nth layer of metal atoms preferably binds to the 2D SiGe ($E_{ave} < 0$)

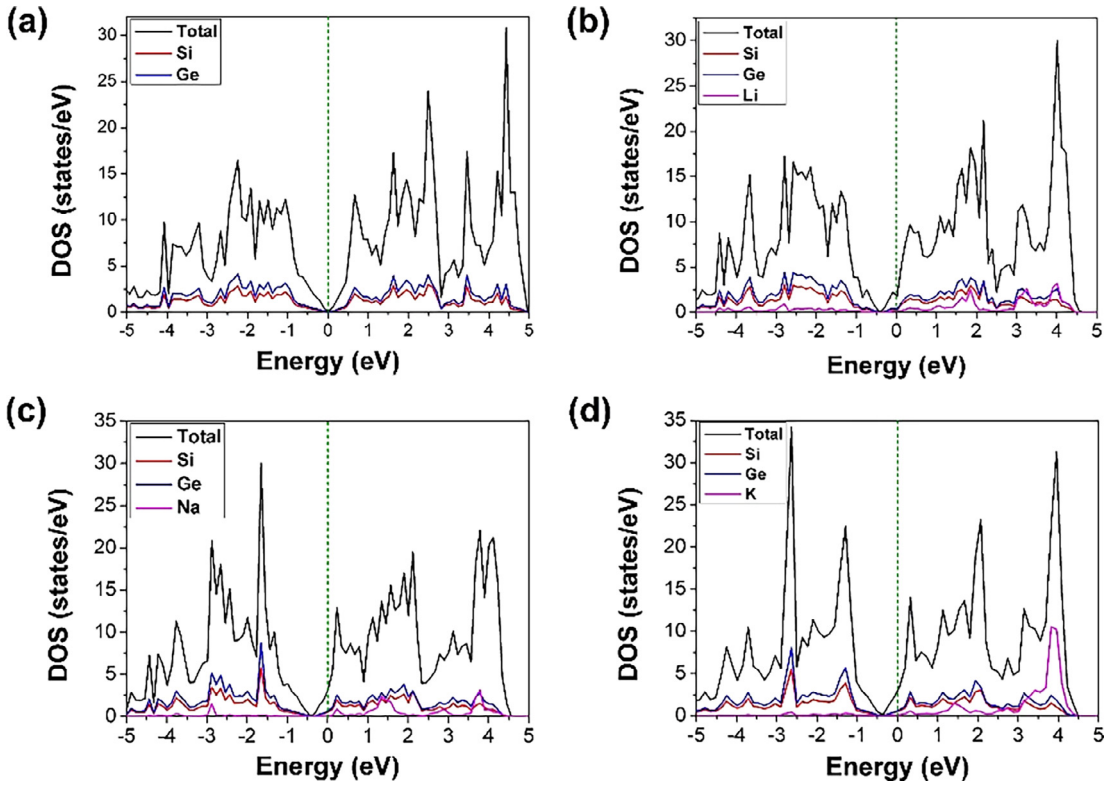

Fig. 3. Total and partial density of states of the sheets of the pristine SiGe (a), $Li_{0.11}SiGe$ (b), $Na_{0.11}SiGe$ (c), and $K_{0.11}SiGe$ (d). The Fermi level is set to zero energy.

or cluster themselves ($E_{ave} > 0$) [8,75,76]. In the first adsorption layer, metal atoms adsorbed to the most stable H sites. The E_{ave} of Li atoms in the first layer was −0.91 eV. The adsorption of the second layer of Li, however, caused an unfavorable rearrangement of the Si–Ge bonds of the 2D SiGe. The resulting distortion of the 2D SiGe was irreversible (Fig. S4). Hence, only a single layer of Li atoms could adsorb on the 2D SiGe. For the adsorption of Na, the E_{ave}s in three consecutive layers were −0.85, −0.039, and 0.06 eV, respectively, indicating the clustering of Na in the third layer. Na atoms in the second and third layers adsorbed on T_{Si} and T_{Ge} sites, respectively. The E_{ave}s of two K layers varied as −0.77 and 0.0075 eV, respectively, so that K atoms in the second layer cluster. Fig. S5 illustrates the adsorption patterns adsorbed with the maximal capacities of metal atoms.

To understand the multilayer adsorption behaviors of Na and K atoms, we evaluated the electron localization functions (ELFs) of the (1 1 0) sections of the SiGe sheets adsorbed with three Na layers and two K layers (Fig. 6). In the ELF plot of the third layer of Na, a significant portion of electrons resided between Na atoms, indicating the strong bonding between them. The PDOS of Na_xSiGe (Fig. 6b) near the Fermi level had a little contribution from Na atoms in the first layer, indicating the weak repulsion between SiGe and Na. The Na atoms in the subsequent adsorption layers however largely contributed to the DOS near the Fermi level. The strong repulsion between SiGe and Na decreased the adsorption strengths of Na atoms in the second and third layers. Similarly, K atoms in the second layer tended to form metal clusters. The ELF of the K second layer shows that electrons are more localized, presumably due to the electron transfer from the spherical *s* orbital of K to the nonspherical *p* or *d* orbital of Ge. In the PDOS of K_xSiGe (Fig. 6d), even the first layer of K atoms gave some contributions in the vicinity of the Fermi level, governing the repulsion between SiGe and K atoms. This repulsive interaction weakened the adsorption strength of the K atoms in the first layer, compared to those of the Li

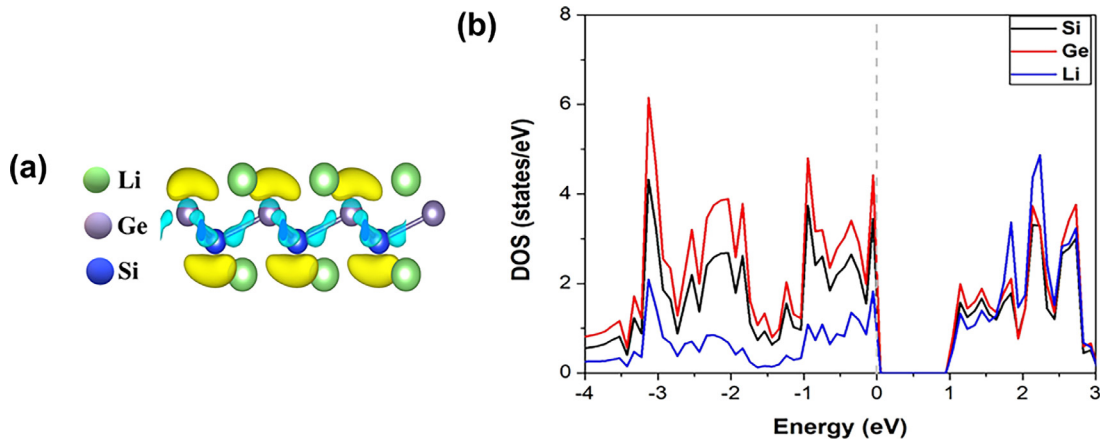

Fig. 4. (a) Differential charge densities of the fully lithiated SiGe sheet. The cyan and yellow areas represent electron loss and gain, respectively. (b) PDOS of $Li_{2.0}SiGe$ representing a broadening of the band gap.

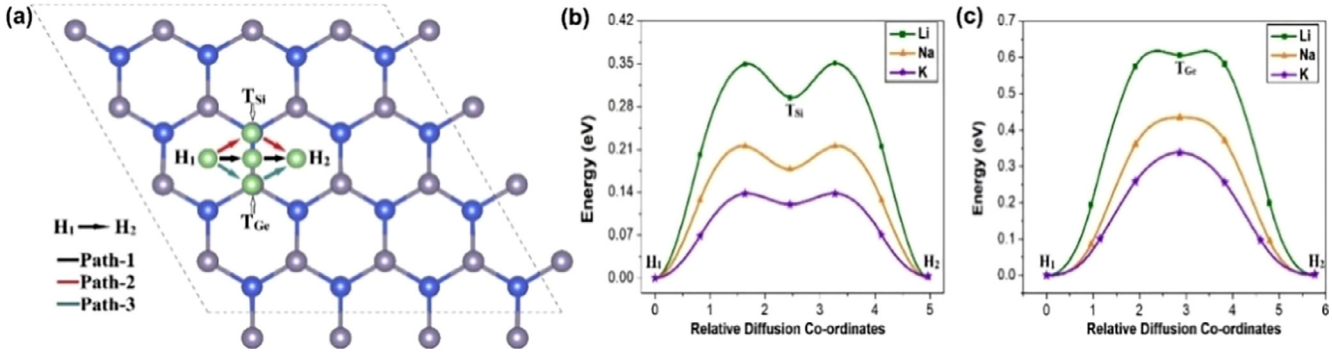

Fig. 5. (a) Migration pathways of Li/Na/K metal atoms and the corresponding minimum energy profiles along (b) Path-2 and (c) Path-3.

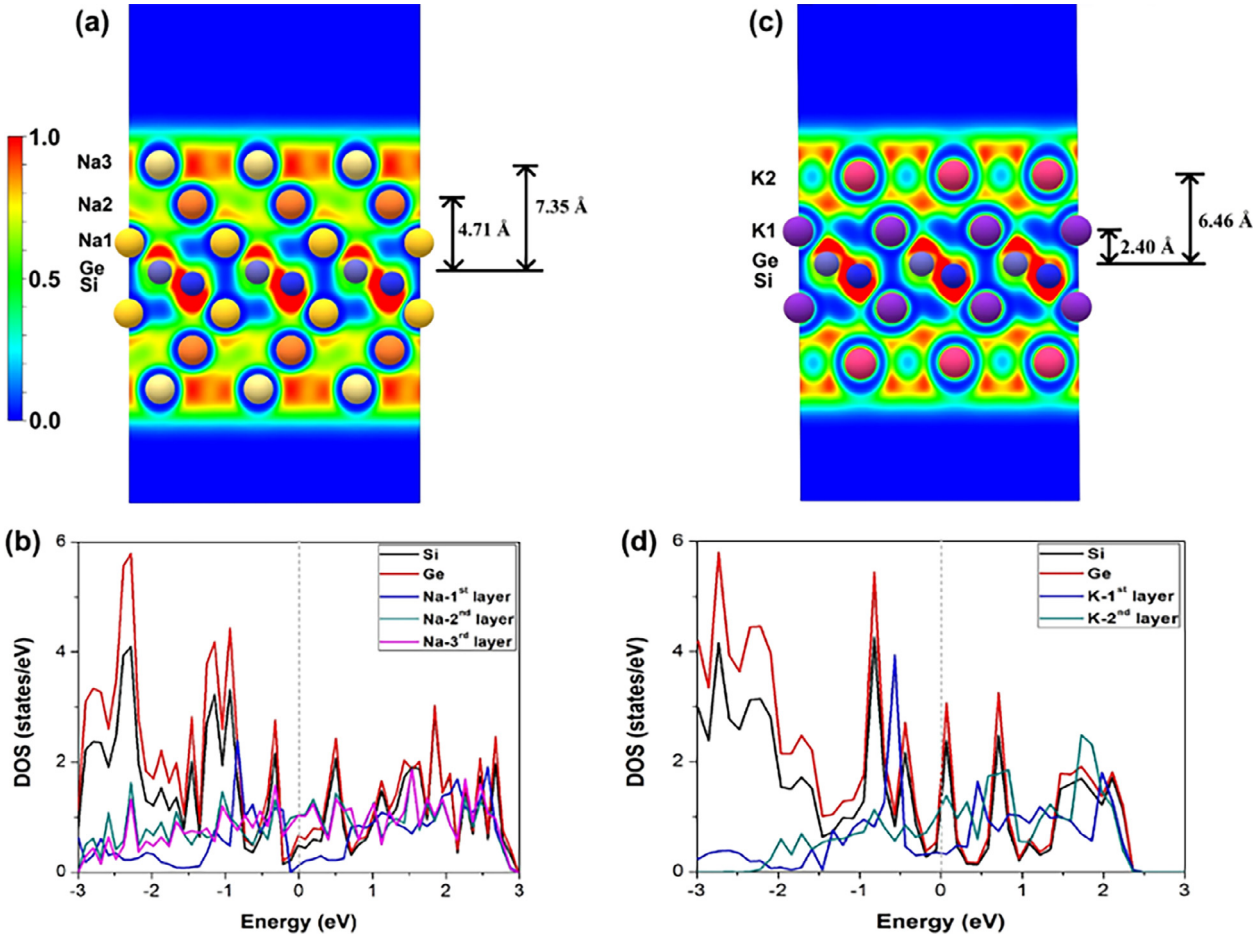

Fig. 6. Electron localization functions calculated for the (1 1 0) cross-sections of the multilayers of Na (a) and K (c) atoms adsorbed on the SiGe sheet. The corresponding PDOSs of the SiGe sheets adsorbed with metal layers are shown in (b) and (d).

and Na atoms in the first layer. In addition, Na and K atoms in the outermost layers were too far from SiGe (by distances of 7.35 and 6.46 Å, respectively) to be chemically bonded.

The ionic intercalation potential is another crucial factor which determines the energy density of the electrode material. The voltage and capacity were evaluated by considering the common half-cell reaction vs. M/M^+:

$$SiGe + xM^+ + xe^- \leftrightarrow M_xSiGe$$

We studied the stabilities of the intermediate phases (M_xSiGe) relative to two end structures: the pristine 2D SiGe and 2D SiGe loaded with the maximal capacity of Li, Na, or K (Li_2SiGe, Na_4SiGe, or K_2SiGe, respectively). To construct a formation energy convex hull, we generated all the symmetrically distinct configurations at different metal concentrations by using the Pymatgen package [77]. The formation energy, ΔE_{form}, was given by [28]

$$\Delta E_{form} = E_{M_xSiGe} - \left[\frac{xE_{M_ySiGe} + (y-x)E_{SiGe}}{y}\right] \quad (6)$$

where x and y are the intermediate and maximum concentrations of metal atoms per unit cell of 2D SiGe, respectively. E_{SiGe}, E_{M_xSiGe}, and E_{M_ySiGe} are the total energies of the pristine 2D SiGe, and 2D SiGe adsorbed with x and y metal atoms, respectively. Fig. 7a shows the convex hull of the formation energy where the stable phases are lying on the hull. For Li, the intermediate phases of M_xSiGe had xs of 0.00, 0.33, 1.00, and 2.00. Similarly, x values of Na were 0.00, 0.33, 2.00, and 4.00

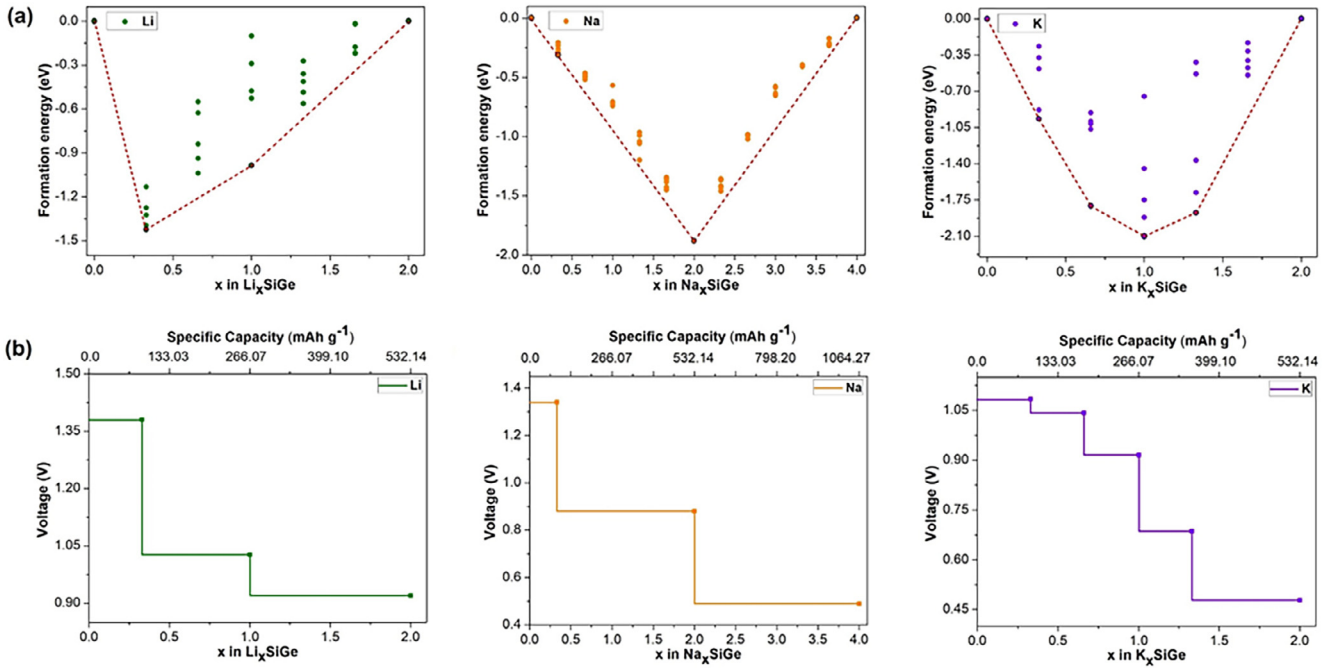

Fig. 7. (a) Formation energies at different Li/Na/K compositions and (b) corresponding electrode potential profiles (vs M/M^+) of Li_xSiGe, Na_xSiGe, and K_xSiGe.

and x values of K were 0.00, 0.33, 0.66, 1.00, 1.33, and 2.00. These compositions were then used to compute the voltage, V [78,79], given by

$$V = -\frac{E(M_{x_2}SiGe) - E(M_{x_1}SiGe) - (x_2 - x_1)E_{M_{bulk}}}{(x_2 - x_1)e} \quad (7)$$

where $E(M_{x_2}SiGe)$ and $E(M_{x_1}SiGe)$ are the total energies of the 2D SiGe adsorbed with x_2 and x_1 metal atoms, respectively, and $E_{M_{bulk}}$ is the energy per atom of the bulk metal. The calculated voltages for Li_xSiGe were in the range of 0.92–1.38 V, with an average open circuit voltage (OCV) of 1.15 V. The 2D Na_xSiGe and K_xSiGe had electrode potentials of 0.49–1.34 V and 0.47–1.08 V, with average OCVs of 0.91 V and 0.78 V, respectively. The calculated voltages were within the range found for graphite (0.10 V) [80] and TiO_2 (1.50 V) anodes [81].

The present 2D SiGe held the maxima of 2 Li, 4 Na, and 2 K atoms per unit cell (Fig. 7) giving the stoichiometries of Li_2SiGe, Na_4SiGe, and K_2SiGe, respectively. The theoretical capacity, C, was given by

$$C = \frac{x_{max}F}{MW_{SiGe}} \quad (8)$$

where x_{max} is the highest concentration of metal atoms in M_xSiGe, F is Faraday constant, and MW_{SiGe} is the molar mass of SiGe. The calculated theoretical capacities of the 2D SiGe for Li, Na and K atoms were 532.13 mA h g^{-1}, 1064.247 mA h g^{-1}, and 532.13 mA h g^{-1}, respectively. These storage capacities are appreciably higher than found for other 2D anodes, such as MXenes [82], group-IV monochalcogenides [31], MoN_2 [68], Ti_3C_2 [83], ScO_2 [84], TiS_3 [72], and VS_2 [85,86]. Table S1 lists the storage capacities of different 2D anode materials.

4. Conclusion

Using the DFT simulation, we systematically studied the structural, electronic, and electrochemical properties of the 2D sheet of SiGe as an anode material for Li/Na/K ion batteries. The present 2D sheet of SiGe was thermally and dynamically stable. The metal atoms preferred to adsorb on the 2D SiGe without the formation of a metal cluster. Due to the charge redistribution, the adsorption of alkali metals enhanced the electrical conductivity of the SiGe sheet. Upon full lithiation, the band gap of the 2D SiGe was reopened, but the fully sodiated and potassiated sheets of SiGe were still metallic. The alkali metal atoms consistently diffused with low diffusion barriers, indicating a fast charging and discharging of the present 2D SiGe. The calculated average OCVs were in the range of those of commercial anode materials. With a high storage performance as well, the present 2D SiGe is a promising material as an anode for Na- and K- ion batteries.

5. Notes

The authors declare no competing financial interest.

Acknowledgment

This study was supported by National Research Foundation Grants funded by the Korean Government (2018R1A2A2A05019776).

Appendix A. Supplementary data

Supplementary data to this article can be found online at https://doi.org/10.1016/j.commatsci.2019.04.039.

References

[1] J.-M. Tarascon, Is lithium the new gold? Nat. Chem. 2 (2010) 510.
[2] W. Tahil, The Trouble with Lithium, Meridian International Research, 2007.
[3] P.K. Nayak, L. Yang, W. Brehm, P. Adelhelm, From lithium-ion to sodium-ion batteries: advantages, challenges, and surprises, Angew. Chem. Int. Ed. 57 (2018) 102–120.
[4] J.-Y. Hwang, S.-T. Myung, Y.-K. Sun, Sodium-ion batteries: present and future, Chem. Soc. Rev. 46 (2017) 3529–3614.
[5] X. Wu, D.P. Leonard, X. Ji, Emerging non-aqueous potassium-ion batteries: challenges and opportunities, Chem. Mater. 29 (2017) 5031–5042.
[6] N. Yabuuchi, K. Kubota, M. Dahbi, S. Komaba, Research development on sodium-ion batteries, Chem. Rev. 114 (2014) 11636–11682.
[7] J.C. Pramudita, D. Sehrawat, D. Goonetilleke, N. Sharma, An initial review of the status of electrode materials for potassium-ion batteries, Adv. Energy Mater. 7 (2017) 1602911.
[8] P. Bhauriyal, A. Mahata, B. Pathak, Graphene-like carbon – nitride monolayer: a potential anode material for Na- and K-ion batteries, J. Phys. Chem. C 122 (2018) 2481–2489.
[9] S. Komaba, T. Hasegawa, M. Dahbi, K. Kubota, Potassium intercalation into graphite to realize high-voltage/high-power potassium-ion batteries and potassium-ion capacitors, Electrochem. Commun. 60 (2015) 172–175.
[10] C.K. Chan, H. Peng, G. Liu, K. Mcilwrath, X.F. Zhang, R.A. Huggins, Y. Cui, High-

performance lithium battery anodes using silicon nanowires, Nat. Nanotechnol. 3 (2008) 31–35.
[11] M.-H. Park, K. Kim, J. Kim, J. Cho, Flexible dimensional control of high-capacity li-ion-battery anodes: from 0D hollow to 3D porous germanium nanoparticle assemblies, Adv. Mater. 22 (2010).
[12] Y. Yang, S. Liu, X. Bian, J. Feng, Y. An, C. Yuan, Morphology- and porosity-tunable synthesis of 3D nanoporous sige alloy as a high-performance lithium-ion battery anode, ACS Nano 12 (2018) 2900–2908.
[13] W. Li, X. Sun, Y. Yu, Ge- Si-, Sn-based anode materials for lithium-ion batteries: from structure design to electrochemical performance, Small Methods 1 (2017) 1600037.
[14] M. Amato, M. Palummo, S. Ossicini, SiGe nanowires: structural stability, quantum confinement, and electronic properties, Phys. Rev. B 80 (2009) 235333.
[15] S. Ciraci, I.P. Batra, Strained Si/Ge superlattices: structural stability, growth, and electronic properties, Phys. Rev. B 38 (1988) 1835–1848.
[16] G. Katsaros, P. Spathis, M. Stoffel, F. Fournel, M. Mongillo, V. Bouchiat, F. Lefloch, A. Rastelli, O.G. Schmidt, S.D. Franceschi, Hybrid superconductor–semiconductor devices made from self-assembled SiGe nanocrystals on silicon, Nat. Nanotechnol. 5 (2010) 458–464.
[17] J. Wang, N. Du, H. Zhang, J. Yu, D. Yang, Cu–Ge core–shell nanowire arrays as three-dimensional electrodes for high-rate capability lithium-ion batteries, J. Mater. Chem. 22 (2012) 1511–1515.
[18] J. Wang, N. Du, Z. Song, H. Wu, H. Zhang, D. Yang, Synthesis of SiGe-based three-dimensional nanoporous electrodes for high performance lithium-ion batteries, J. Power Sour. 229 (2013) 185–189.
[19] Y. Zhang, N. Du, C. Xiao, S. Wu, Y. Chen, Y. Lin, J. Jiang, Y. He, D. Yang, Simple synthesis of SiGe@C porous microparticles as high-rate anode materials for lithium-ion batteries, RSC Adv. 7 (2017) 33837–33842.
[20] W.-J. Zhang, A review of the electrochemical performance of alloy anodes for li-thium-ion batteries, J. Power Sour. 196 (2011) 13–24.
[21] J. Yu, N. Du, J. Wang, H. Zhang, D. Yang, SiGe porous nanorod arrays as high-performance anode materials for lithium-ion batteries, J. Alloys Compd. 577 (2013) 564–568.
[22] H. Kim, Y. Son, C. Park, M.-J. Lee, M. Hong, J. Kim, M. Lee, J. Cho, H.C. Choi, Germanium silicon alloy anode material capable of tunable overpotential by nanoscale Si segregation, Nano Lett. 15 (2015).
[23] T. Song, H. Cheng, H. Choi, J.-H. Lee, H. Han, D.H. Lee, D.S. Yoo, M.-S. Kwon, J.-M. Choi, S.G. Doo, H. Chang, J. Xiao, Y. Huang, W.I. Park, Y.-C. Chung, H. Kim, J.A. Rogers, U. Paik, Si/Ge double-layered nanotube array as a lithium ion battery anode, ACS Nano 6 (2012) 303–309.
[24] W. Li, Y. Yang, G. Zhang, Y.-W. Zhang, Ultrafast and directional diffusion of lithium in phosphorene for high-performance lithium-ion battery, Nano Lett. 15 (2015) 1691–1697.
[25] V.V. Kulish, O.I. Malyi, C. Persson, P. Wu, Phosphorene as an anode material for Na-ion batteries: a first-principles study, Phys. Chem. Chem. Phys. 17 (2015) 13921–13928.
[26] H.R. Jiang, W. Shyy, M. Liu, L. Wei, M.C. Wu, T.S. Zhao, Boron phosphide monolayer as a potential anode material for alkali metal-based batteries, J. Mater. Chem. A 5 (2017) 672–679.
[27] D. Rao, L. Zhang, Z. Meng, X. Zhang, Y. Wang, G. Qiao, X. Shen, H. Xia, J. Liu, R. Lu, Ultrahigh energy storage and ultrafast ion diffusion in borophene-based anodes for rechargeable metal ion batteries, J. Mater. Chem. A 5 (2017) 2328–2338.
[28] V. Shukla, R.B. Araujo, N.K. Jena, R. Ahuja, The curious case of two dimensional Si_2BN: a high-capacity battery anode material, Nano Energy 41 (2017) 251–260.
[29] H. Wang, M. Wu, X. Lei, Z. Tian, B. Xu, K. Huang, C. Ouyang, Siligraphene as a promising anode material for lithium-ion batteries predicted from first-principles calculations, Nano Energy 49 (2018) 67–76.
[30] F. Li, Y. Qu, M. Zhao, Germanium sulfide nanosheet: a universal anode material for alkali metal ion batteries, J. Mater. Chem. A 4 (2016) 8905–8912.
[31] A. Sannyal, Z. Zhang, X. Gao, J. Jang, Two-dimensional sheet of germanium selenide as an anode material for sodium and potassium ion batteries: First-principles simulation study, Comput. Mater. Sci. 154 (2018) 204–211.
[32] A. Huang, X. Sun, S. Dong, Tin monooxide monolayer as promising anode materials for recharge ion batteries, Int. J. Electrochem. Sci. 12 (2017) 10534–10541.
[33] C.-S. Liu, X.-L. Yang, J. Liu, X.-J. Ye, Theoretical prediction of two-dimensional SnP_3 as a promising anode material for Na-ion batteries, ACS Appl. Energy Mater. 1 (2018) 3850–3859.
[34] G.A. Tritsaris, E. Kaxiras, S. Meng, E. Wang, Adsorption and diffusion of lithium on layered silicon for Li-ion storage, Nano Lett. 13 (2013) 2258–2263.
[35] B. Mortazavi, A. Dianat, G. Cuniberti, T. Rabczuk, Application of silicene, germanene and stanene for Na or Li ion storage: a theoretical investigation, Electrochim. Acta 213 (2016) 865–870.
[36] J. Zhu, U. Schwingenschlögl, Silicene for Na-ion battery applications, 2D Mater. 3 (2016) 035012.
[37] G. Liu, X.L. Lei, M.S. Wu, B. Xu, C.Y. Ouyang, Comparison of the stability of free-standing silicene and hydrogenated silicene in oxygen: a first principles investigation, J. Phys.: Condens. Matter 26 (2014) 355007.
[38] G. Liu, S.B. Liu, B. Xu, C.Y. Ouyang, H.Y. Song, First-principles study of the stability of free-standing germanene in oxygen atmosphere, J. Appl. Phys. 118 (2015) 124303.
[39] H. Zhou, M. Zhao, X. Zhang, W. Dong, X. Wang, H. Bu, A. Wang, First-principles prediction of a new Dirac-fermion material: silicon germanide monolayer, J. Phys.: Condens. Matter 25 (2013) 395501.
[40] P. Jamdagni, A. Kumar, A. Thakur, R. Pandey, P. Ahluwalia, Stability and electronic properties of SiGe-based 2D layered structures, Mater. Res. Express 2 (2015) 016301.
[41] W.X. Zhang, Y.B. Wang, P. Zhao, C. He, Tuning the electronic and magnetic properties of graphene-like SiGe hybrid nanosheets by surface functionalization, Phys. Chem. Chem. Phys. 18 (2016) 26205–26212.
[42] P.E. Blochl, Projector augmented-wave method, Phys. Rev. B 50 (1994) 17953–17979.
[43] J.P. Perdew, K. Burke, M. Ernzerhof, Generalized gradient approximation made simple, Phys. Rev. Lett. 77 (1996) 3865–3868.
[44] S. Grimme, Semiempirical GGA-type density functional constructed with a long-range dispersion correction, J. Comput. Chem. 27 (2006) 1787–1799.
[45] P. Ganesh, J. Kim, C. Park, M. Yoon, F.A. Reboredo, P.R.C. Kent, Binding and diffusion of lithium in graphite: quantum Monte Carlo benchmarks and validation of van der Waals density functional methods, J. Chem. Theory Comput. 10 (2014) 5318–5323.
[46] A. Togo, I. Tanaka, First principles phonon calculations in materials science, Scr. Mater. 108 (2015) 1–5.
[47] H.J. Monkhorst, J.D. Pack, Special points for Brillonin-zone integrations, Phys. Rev. B 13 (1976) 5188–5192.
[48] W. Tang, E. Sanville, G. Henkelman, A grid-based Bader analysis algorithm without lattice bias, J. Phys.: Condens. Matter 21 (2009) 084204.
[49] E. Sanville, S.D. Kenny, R. Smith, G. Henkelman, Improved grid-based algorithm for bader charge allocation, J. Comput. Chem. 28 (2006) 899–908.
[50] G. Henkelman, A. Arnaldsson, H. Jonsson, A fast and robust algorithm for Bader decomposition of charge density, Comput. Mater. Sci. 36 (2006) 354–360.
[51] G. Henkelman, B.P. Uberuaga, H. Jónsson, A climbing image nudged elastic band method for finding saddle points and minimum energy paths, J. Chem. Phys. 113 (2000) 9901–9904.
[52] G. Henkelman, H. Jónsson, Improved tangent estimate in the nudged elastic band method for finding minimum energy paths and saddle points, J. Chem. Phys. 113 (2000) 9978–9985.
[53] G. Kresse, J. Furthmüller, Efficient iterative schemes for ab initio total-energy calculations using a plane-wave basis set, Phys. Rev. B 54 (1996) 11169–11186.
[54] G. Kresse, D. Joubert, From ultrasoft pseudopotentials to the projector augmented-wave method, Phys. Rev. B 59 (1999) 1758–1775.
[55] X. Gonze, C. Lee, Dynamical matrices, born effective charges, dielectric permittivity tensors, and interatomic force constants from density-functional perturbation theory, Phys. Rev. B 55 (1997) 10355–10368.
[56] S. Karmakar, C. Chowdhury, A. Datta, Two-dimensional group IV mono-chalcogenides: anode materials for Li-Ion batteries, J. Phys. Chem. C 120 (2016) 14522–14530.
[57] H. Sahin, F.M. Peeters, Adsorption of alkali, alkaline-earth, and 3d transition metal atoms on silicene, Phys. Rev. B 87 (2013) 085423.
[58] K.S. Novoselov, A.K. Geim, S.V. Morozov, D. Jiang, M.I. Katsnelson, I.V. Grigorieva, S.V. Dubonos, A.A. Firsov, Two-dimensional gas of massless Dirac fermions in graphene, Nature 438 (2005) 197–200.
[59] J.C. Garcia, D.B.d. Lima, L.V.C. Assali, J.a.F. Justo, Group IV graphene- and graphane-like nanosheets, J. Phys. Chem. C 115 (2011) 13242–13246.
[60] N.D. Drummond, V. Zolyomi, V.I. Falko, Electrically tunable band gap in silicene, Phys. Rev. B 85 (2012) 075423.
[61] Z. Ni, Q. Liu, K. Tang, J. Zheng, J. Zhou, R. Qin, Z. Gao, D. Yu, J. Lu, Tunable bandgap in silicene and germanene, Nano Lett. 12 (2012) 113–118.
[62] S. Cahangirov, M. Topsakal, E. Akturk, H. Sahin, S. Ciraci, Two- and one-dimensional honeycomb structures of silicon and germanium, Phys. Rev. Lett. 102 (2009) 236804.
[63] G.-C. Guo, D. Wang, X.-L. Wei, Q. Zhang, H. Liu, W.-M. Lau, L.-M. Liu, First-principles study of phosphorene and graphene heterostructure as anode materials for rechargeable Li batteries, J. Phys. Chem. Lett. 6 (2015) 5002–5008.
[64] A. Samad, M. Noor-A-Alam, Y.-H. Shin, First principles study of a SnS_2/graphene heterostructure: a promising anode material for rechargeable Na ion batteries, J. Mater. Chem. A 4 (2016) 14316–14323.
[65] Q. Sun, Y. Dai, Y. Ma, T. Jing, W. Wei, B. Huang, Ab initio prediction and characterization of Mo_2C monolayer as anodes for lithium-ion and sodium-ion batteries, J. Phys. Chem. Lett. 7 (2016) 937–943.
[66] D. Çakır, C. Sevik, O.g. Gulseren, F.M. Peeters, Mo_2C as a high capacity anode material: a first-principles study, J. Mater. Chem. A 4 (2016) 6029–6035.
[67] A. Urban, D.-H. Seo, G. Ceder, Computational understanding of Li-ion batteries, NPJ Comput. Mater. 2 (2016) 16002.
[68] X. Zhang, Z. Yu, S.-S. Wang, S. Guan, H.Y. Yang, Y. Yao, S.A. Yang, Theoretical prediction of MoN_2 monolayer as a high capacity electrode material for metal ion batteries, J. Mater. Chem. A 4 (2016) 15224–15231.
[69] W. Wan, Q. Zhang, Y. Cui, E. Wang, First principles study of lithium insertion in bulk silicon, J. Phys.: Condens. Matter 22 (2010) 415501.
[70] M.V. Koudriachova, N.M. Harrison, S.W.d. Leeuw, Effect of diffusion on lithium intercalation in titanium dioxide, Phys. Rev. Lett. 86 (2001) 1275–1278.
[71] M. Wagemaker, R.v.d. Krol, A.P.M. Kentgens, A.A.v. Well, F.M. Mulder, Two phase morphology limits lithium diffusion in TiO_2 (Anatase): A ^{7}Li MAS NMR study, J. Am. Chem. Soc. 123 (2001) 11454–11461.
[72] J. Wu, D. Wang, H. Liu, W.-M. Lau, L.-M. Liu, An ab initio study of TiS_3: a promising electrode material for rechargeable Li and Na ion batteries, RSC Adv. 5 (2015) 21455–21463.
[73] T. Yu, Z. Zhao, L. Liu, S. Zhang, H. Xu, G. Yang, TiC_3 monolayer with high specific capacity for sodium-ion batteries, J. Am. Chem. Soc. 140 (2018) 5962–5968.
[74] S. Wang, B. Yang, H. Chen, E. Ruckenstein, Popgraphene: a new 2D planar carbon allotrope composed of 5–8–5 carbon rings for high performance lithium-ion battery anodes from bottom-up programming, J. Mater. Chem. A 6 (2018) 6815–6821.
[75] M. Liu, A. Kutana, Y. Liu, B.I. Yakobson, First-principles studies of Li nucleation on graphene, J. Phys. Chem. Lett. 5 (2014) 1225–1229.

[76] A.M. Garay-Tapia, A.H. Romero, V. Barone, Lithium adsorption on graphene: from isolated adatoms to metallic sheets, J. Chem. Theory Comput. 8 (2012) 1064–1071.
[77] S.P. Ong, W.D. Richards, A. Jain, G. Hautier, M. Kocher, S. Cholia, D. Gunter, V.L. Chevrier, K.A. Persson, G. Ceder, Python Materials Genomics (pymatgen): a robust, open-source python library for materials analysis, Comput. Mater. Sci. 68 (2013) 314–319.
[78] M.K. Aydinol, A.F. Kohan, G. Ceder, K. Cho, J. Joannopoulos, Ab initio study of lithium intercalation in metal oxides and metal dichalcogenides, Phys. Rev. B 56 (1997) 1354–1365.
[79] X. Lv, W. Wei, Q. Sun, L. Yu, B. Huang, Y. Dai, Sc_2C as a promising anode material with high mobility and capacity: a first-principles study, ChemPhysChem 18 (2017) 1627–1634.
[80] J.R. Dahn, Phase diagram of Li_xC_6, Phys. Rev. B 44 (1991) 9170–9177.
[81] Z. Yang, D. Choi, S. Kerisit, K.M. Rosso, D. Wang, J. Zhang, G. Graff, J. Liu, Nanostructures and lithium electrochemical reactivity of lithium titanites and titanium oxides: a review, J. Power Sour. 192 (2009) 588–598.
[82] Y. Xie, Y. DallAgnese, M. Naguib, Y. Gogotsi, M.W. Barsoum, H.L. Zhuang, P.R.C. Kent, Prediction and characterization of MXene nanosheet anodes for non-lithium-ion batteries, ACS Nano 8 (2014) 9606–9615.
[83] D. Er, J. Li, M. Naguib, Y. Gogotsi, V.B. Shenoy, Ti_3C_2 MXene as a high capacity electrode material for metal (Li, Na, K, Ca) ion batteries, ACS Appl. Mater. Interfaces 6 (2014) 11173–11179.
[84] Z. Liu, H. Deng, S. Zhang, W. Hu, F. Gao, A first-principles investigation of the ScO_2 monolayer as the cathode material for alkali metalion batteries, J. Mater. Chem. A 6 (2018) 3171–3180.
[85] Y. Jing, Z. Zhou, C.R. Cabrera, Z. Chen, Metallic VS_2 monolayer: a promising 2D anode material for lithium ion batteries, J. Phys. Chem. C 117 (2013) 25409–25413.
[86] D.B. Putungan, S.-H. Lin, J.-L. Kuo, Metallic VS_2 monolayer polytypes as potential sodium-ion battery anode via ab initio random structure searching, ACS Appl. Mater. Interfaces 8 (2016) 18754–18762.